Volume 401, 25 April 2016 ISSN 1387-3806

ELSEVIER

INTERNATIONAL JOURNAL OF

Mass Spectrometry

"A large-radius high-mass-resolution multiple-collector isotope ratio mass spectrometer for analysis of rare isotopologues of O_2, N_2, CH_4 and other gases"

Corresponding Author:
Prof. Edward Young

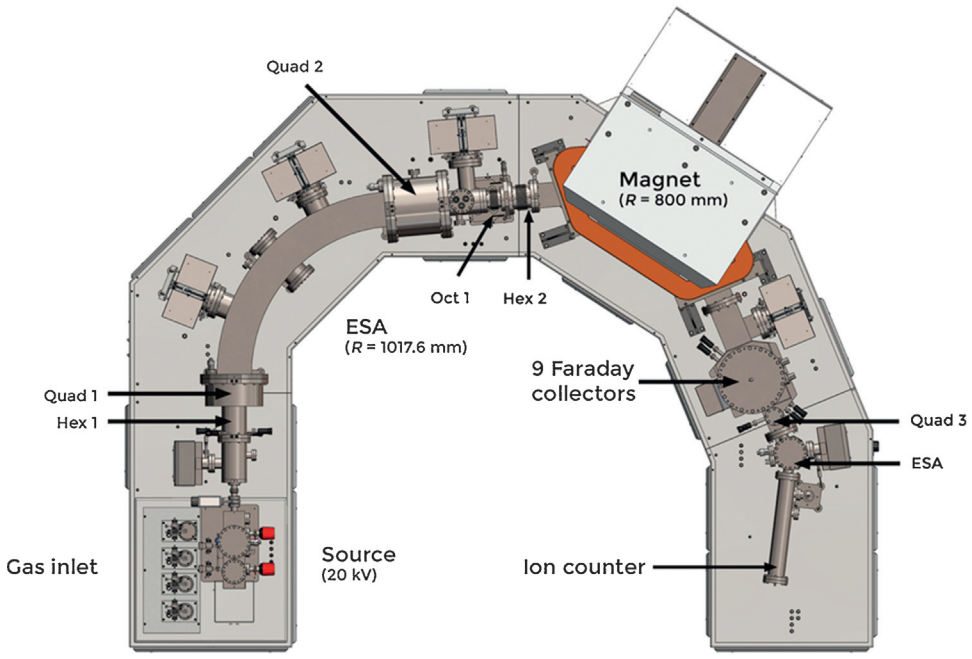

On-line Access via: www.elsevier.com/locate/ijms

International Journal of Mass Spectrometry 401 (2016) 1–10

Contents lists available at ScienceDirect

International Journal of Mass Spectrometry

journal homepage: www.elsevier.com/locate/ijms

A large-radius high-mass-resolution multiple-collector isotope ratio mass spectrometer for analysis of rare isotopologues of O_2, N_2, CH_4 and other gases

Edward D. Young [a,*], Douglas Rumble III [b], Philip Freedman [c], Mark Mills [c]

[a] Department of Earth, Planetary, and Space Sciences, University of California Los Angeles, CA 90095-1567, USA
[b] Geophysical Laboratory, 5251 Broad Branch Rd. NW, Washington, DC 20015-1305, USA
[c] Nu Instruments Limited, Unit 74 Clywedog Road South, Wrexham LL139XS, UK

ARTICLE INFO

Article history:
Received 14 August 2015
Received in revised form 7 January 2016
Accepted 20 January 2016
Available online 10 March 2016

Keywords:
Isotope ratios
Mass spectrometry
Mass-resolution
Rare isotopologues
Methane
Oxygen

ABSTRACT

We describe a unique and novel isotope ratio mass spectrometer (IRMS), the *Panorama*, developed explicitly for high-mass-resolution analysis of isotopologue ratios of gas samples. The double-focussing instrument routinely operates at a mass resolving power of 40,000 with a maximum useful MRP of ~80,000. The instrument achieves this exceptional MRP for a multi-collector using a Matsuda ion optical design with an ESA radius of 1018 mm and a magnetic sector radius of 800 mm. Collectors comprise 9 Faraday cups and a single channel of ion counting each with continuously variable collector slits. First results demonstrate both accuracy and precision comparable to, and in some cases, surpassing, other gas-source multi-collector IRMS instruments for singly-substituted species. For example, accurate bulk D/H and $^{13}C/^{12}C$ for methane gas measured with CH_4 as the analyte are measured simultaneously with internal precision of 0.02–0.04‰ (1 std error) and ~0.006‰ (1 se), respectively. Ion counting with continuous rebalancing of sample and standard gases permits high-precision measurements of rare, multiply-substituted isotopologues with relative abundances as small as ~0.1 ppm. In the case of methane, both $^{13}CH_3D/^{12}CH_4$ and $^{12}CH_2D_2/^{12}CH_4$ ratios are measured with precision of ~0.1‰ and ~0.5‰, respectively. Accuracy of the multiply-substituted species measurements is demonstrated using isotope ratio mixing experiments. The ability to measure both $\Delta^{13}CH_3D$ and ΔCH_2D_2 (‰ variations relative to the stochastic reference frame) provides heretofore unmatched capabilities to identify kinetic reaction pathways, isotope fractionation during transport, mixing, as well as temperatures of formation for methane gas. The high-resolution instrument can be used for a wide variety of applications. For example, it easily resolves $^{36}Ar^+$ from $^{18}O^{18}O^+$ for oxygen bond-ordering studies. It also easily resolves $^{14}N^{16}O+$ from $^{15}N^{15}N+$ for measurements of the doubly-substituted N_2 species.

1. Introduction

Gas-source magnetic-sector isotope-ratio mass spectrometers (IRMSs) have been the primary tool for stable isotope analysis of gases dating back to Alfred O. Nier's original design in 1947 [1]. While numerous improvements followed, including addition of more collectors [2] and enhancements in vacuum systems and gas delivery [3,4], the basic design remained largely unchanged until very recently. Virtually all gas-source multiple-collector isotope ratio mass spectrometers in use today are single-focusing magnetic sector instruments with a radius, R, of ≤250 mm and a dispersion, D, of ≤~500 mm ($D \sim 2R$ for stigmatic focusing and unit magnification [5]), similar to the original Nier single-focusing design with $R = 200$ mm. Mass resolving power, MRP, is $\sim D/i$, where i is the image of the ion beam width defined at the entrance to the spectrometer. Gas-source IRMS instruments typically have i of order 0.5 mm. The MRP of these instruments is therefore no greater than ~1000. The requirement for flat-top ion beam peaks for isotope ratio analysis limits the operational mass resolution to at most ~1/3 MRP and means that an MRP of ~1000 or less corresponds to a practical resolution $m/\Delta m$ of 300 or less. As a consequence, while dynamic gas-source instruments provide

* Corresponding author. Tel.: +1 8185328817.
E-mail addresses:
eyoung@epss.ucla.edu (E.D. Young), drumble@carnegiescience.edu (D. Rumble III), phil.freedman@nu-ins.com (P. Freedman), Mark.Mills@nu-ins.com (M. Mills).

http://dx.doi.org/10.1016/j.ijms.2016.01.006
1387-3806/

unparalleled precision, they have been severely restricted in their application by their inability to resolve species with the same integer mass. This in turn renders them incapable of measuring multiply-substituted isotopologues, with some notable exceptions, that have great potential in the geological and allied sciences [6,7].

This stagnation in gas-source IRMS designs contrasts with that of other isotope-ratio mass spectrometers. Beginning several decades ago, larger geometries with magnetic sector radii of order of 1 m were utilized for multiple-collection secondary ion mass spectrometry (SIMS) [8,9] in order to resolve molecular ion interferences (e.g., hydrides). A large-geometry multiple-collector inductively-coupled plasma-source mass spectrometer (MC-ICPMS) has also appeared in recent years for the same purpose [10]. Achieving mass resolving powers of >10,000 is relatively common in multi-collection isotope ratio mass spectrometry but not for gas-source IRMS instruments. Until now there has been no large-geometry gas-source IRMS instrument.

The energy spread of ions entering the magnetic sector limits its mass resolution, necessitating an energy sector for high mass resolution. Although double-focusing (electrostatic analyzer combined with a magnetic sector) mass spectrometers date back to Dempster [11], and a gas-source double-focusing instrument was built by Johnson and Nier [12,13], with few exceptions (e.g., the Dupont 491 from the 1970s), double-focusing has been virtually absent among commercially-available gas-source instruments historically. A modern double-focusing gas-source mass spectrometer was introduced in 2012, the 253 Ultra (Thermo Scientific) [14] that represents a significant increase in MRP over the traditional single-focusing designs. It is a modification of an existing MC-ICPMS with a magnetic sector radius of 230 mm. The radius of the magnetic sector, and therefore the dispersion/magnification ratio is typical of earlier instruments. However, by virtue of a very narrow entrance (source) slit width of 5 μm, an MRP of up to 27,000 has been reported [14] while sensitivities required for high-precision isotope ratios measurements are obtained with an operational MRP of ~16,000–17,000 [15].

The multiple isotopic species of methane gas provide a useful point of reference for comparing the capabilities of the IRMS instruments described here. For example, with the 253 Ultra described above, H_2O^+ is easily resolved from $^{13}CH_3D^+$ ($m/\Delta m = 594$), allowing for measurements of the latter free of interference from ubiquitous water. However, direct measurement of $^{13}CH_4^+/^{12}CH_4^+$ to obtain the bulk $^{13}C/^{12}C$ ratio and $^{12}CH_3D^+/^{12}CH_4^+$ to obtain the bulk D/H of the methane, while possible with care, is hampered by the inability to simultaneously resolve $^{12}CH_3D^+$ from the lower mass $^{13}CH_4^+$ ($m/\Delta m = 5830$) and the higher mass $^{12}CH_5^+$ adduct ion ($m/\Delta m = 11{,}006$) formed in the electron impact source by reactions like $CH_4^+ + CH_4 \rightarrow CH_5^+ + CH_3$ [16]. As a result, corrections for the presence of multiple species in each ion beam are required. More difficult problems arise for measurements of the relative abundances of the two doubly-substituted mass-18 isotopologues of methane, $^{13}CH_3D$ and CH_2D_2. These two species cannot be resolved with sufficient transmission for isotope ratio analysis even with the upgraded small-geometry design of the 253-Ultra, requiring the two species to be lumped together. This lumping of multiply-substituted species can result in a significant loss of information, as discussed below.

Here we describe the first double-focusing large-radius gas-source IRMS instrument designed expressly to maximize MRP *and* sensitivity for the purpose of measuring the relative abundances of rare, multiply substituted isotopologues. The prototype instrument, the Panorama, was built by Nu Instruments Limited and installed in the stable isotope laboratory in the Department of Earth, Planetary, and Space Sciences at UCLA on 20 March of 2015.

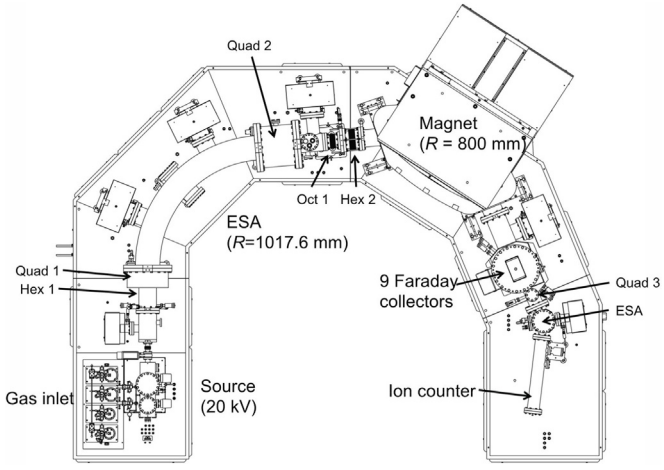

Fig. 1. Layout of the Panorama mass spectrometer with major components labeled.

2. A new high-MRP gas-source IRMS instrument - Panorama

The new instrument is based on the electrostatic sector – quadrupole – magnetic sector optical design by Matusda [17]. The major components of the Panorama include a dual-inlet composed of four variable volume bellows, an electron-impact gas source, a continuously variable source slit, a 72.5°, 1017.6 mm radius electrostatic sector analyzer (ESA), a large quadrupole lense (Quad 2, Fig. 1) between the ESA and magnet, an 85° magnetic sector with a radius of 800 mm, 9 Faraday collectors, and a single channel of ion counting (Fig. 1).

2.1. Mass resolving power and sensitivity

The Panorama has an ion path length of 6.2 m. The total mass dispersion, D, is 630 mm with a magnification of 0.448. The instrument operates routinely at an MRP of ~40,000 or greater, measured as $M/\Delta M$ where M is mass over charge for the ion beam and ΔM is the 5–95% definition of beam width in mass-to-charge units (we use the 5–95% definition of MRP unless otherwise specified in the text). The MRP of 40,000 corresponds to an effective source slit width, s, of 35 μm using MRP = $D/(Xs)$ where X is the magnification and s is the source slit width with the effects of aberrations ignored. Under these operating conditions there is a threefold reduction in transmission relative to a fully open source slit. Thus far, flat-top peaks with transmission suitable for isotopic ratio measurements are obtained at MRP values as high as ~66,000, with a corresponding effective slit width of 21 μm. The continuously-variable source slit provides complete flexibility in defining MRP. A relatively high accelerating voltage of 15–18 kV (20 kV maximum) is used to reduce acceptance angles at high resolution and enhance transmission.

Matusda showed that the introduction of the large, defocussing, Quad 2 lens between the ESA and magnet can give rise to a large reduction in the second and third order aberrations of a double focusing mass spectrometer. The Quad 2 element focuses through the magnet gap, maximizing transmission, while also maximizing D/X and hence mass resolving power. This is especially important for the gas-source where the ion beams are large in the Y (vertical) direction. This D/X figure of merit for the Panorama is 1406 mm. The ESA-Q-magnet geometry provides for maximum MRP and transmission where multi-collection is also paramount. For comparison, the 253 Ultra gas-source IRMS has a D/X of 405 mm [14], comparable to most gas-source instruments. The Panorama D/X of 1406 mm compares favorably with the largest-geometry

multi-collection SIMS instruments that have typical D/X values of ~1200 to ~1700 [18].

We obtain 84,000 molecules per ion of methane at an MRP of 40,000, corresponding to an entrance slit width of about 35 μm.

2.2. Stability

The magnetic field is controlled by feedback from a field probe. Short-term stability was measured by setting the magnet current to coincide with 50% intensity on the flank of a peak at an MRP of ~50,000. These tests demonstrate drift of ≤10 ppm. For a peak flat equal to the width of the ion beam as defined by the width of the peak flank at an MRP of 50,000, the measured drift over one half hour corresponds to better than half the peak top width. The stability therefore corresponds to better than 0.18 mTh (we use thomsons, Th, where Th = Da/z, z is the integer valance, and Da is a Dalton) at m/z = 18 and 0.3 mTh at m/z = 30 over the course of ½ hour.

Measurements made on the Panorama can consume many hours of run time. Long-term stability is therefore a critical parameter. Long-term stability is dominated by temperature control for this large-geometry instrument. For example, the coefficient of linear expansion for 316 stainless steel is 16 ppm/°C, meaning that a 1° shift in temperature will dominate over the intrinsic stability of the instrument magnet and electronics. The laboratory housing the instrument is controlled to 1/2°. However, we find that the addition of steel covers over the ion drift path of the instrument improves the thermal stability as well as protecting against stray magnetic fields. For runs of up to 26 h duration we find that the peak center obtained by the instrument software typically changes by 5 ppm or less. Peak centering is performed regularly by the software throughout the runs, usually before each block of twenty 30-s cycles.

The overall stability of the instrument suggests that the width of peak flats defined by the width of the collector slits should be of order 20 ppm or greater, or two times the short-term stability, for reliable isotope ratio measurements.

Linearity has been assessed using O_2 gas as the analyte. We obtain ~0.1‰/nA under typical operating conditions.

2.3. Collectors and collector slits

Each of the nine Faraday collectors and the axial ion counter has continuously variable collector slits. The two sides of each of the slits are controlled independently from one another by computer, permitting asymmetrical placement of the slits relative to the collector centers. In combination with the movable Faraday cups, these independently variable slits provide for complete flexibility in selecting multiple positions along the dispersion plane for isotope ratio analysis. The slits can be rotated to control vertical alignment. Access to the discrete dynode electron multiplier (from ETP) is obtained by moving aside the axial beam Faraday collector. Focusing the axial beam to the discrete dynode electron multiplier is achieved with a quadrupole lens and a small ESA positioned just behind the Faraday collectors (Fig. 1).

The usual configuration of the Panorama makes use of 1×10^{11} Ω resistors for the Faraday cup amplifiers. The maximum ion current is $\sim 5 \times 10^{-10}$ amp with these resistors (i.e., 50 V). Swapping resistors is straightforward, requiring no break in vacuum, and we have made use of values ranging from 1×10^{9} Ω to 1×10^{12} Ω for various gases.

Gas-sources with dual inlets turn out to be ideally suited for applications involving electron multipliers although they have been seldom used on these instruments. Measurements on the Panorama are carried out with count rates of ~100 cps to 20,000 cps. Deadtime corrections, although unnecessary here, are applied (25 ns). However, even at higher count rates, the rapid switching between sample and standards reduces the dependence of the accuracy of measurements on deadtime values, which can be limiting in other techniques.

2.4. Mass range

The accessible mass/charge of the instrument at the full accelerating voltage of 20 kV ranges up to ~70, relevant for isotopologue measurements of SO_2. Here the separation between peaks is 9.5 mm, which is greater than the minimum slit-to-slit separation for the collectors of ~8 mm. Lowering the accelerating voltage to 10 kV extends the mass range.

2.5. Gas delivery and vacuum system

Gas is delivered using a dual inlet [3] with sample/standard change-over valves. Four variable volume bellows are included with a range of volumes from 120 ml to 26 ml. Any of the four bellows can be selected as the sample or the standard for an analysis. Precision using the sample/standard changeover assembly in general will depend in part on the quality of the pressure (ion current) balance between sample and standard. The bellows on the Panorama are controlled by the software that permits rebalancing of the ion current for sample and standard ion beams to within ~1% for each measurement cycle (typically every 30 s). In this fashion, extraordinarily long analysis runs of tens of hours are possible with no loss in sample/standard balance. For example, we have carried out 26 h analyses with balance between sample and standard ion beams maintained to within 1% throughout.

The source is pumped by two turbomolecular pumps. The ESA, drift and flight tubes, and collector housing are pumped by ion pumps (Fig. 1) with background pressures in the low 10^{-9} to 10^{-10} mbar range.

3. Example application – methane gas

3.1. Motivation and theory

The propensity of two heavy isotopes (^{13}C or D in this case) to occur in the same molecule of methane is an intra-molecular isotopic indicator of provenance. The phenomenon of multiple rare isotope substitution in gases, also known as "isotope clumping," has been explored recently in atmospheric CO_2 [19,20], in atmospheric O_2 [7], and in CH_4 gas [15]. One of our goals with the Panorama is to extend the applicability of this powerful tracer by providing the means to measure two rare isotopologues in methane gas simultaneously. The use of two rare species overcomes the limitations in interpretations that are based on the assumption of thermal equilibrium.

The concept of isotope clumping is understood relative to the null condition of the purely stochastic distribution of isotopologues of a molecule. In the case of methane one is concerned with the fraction of carbon that is the heavy isotope, ^{13}C:

$$X(^{13}C) = \frac{^{13}C}{^{13}C+^{12}C} \quad (1)$$

and the fraction of the hydrogen isotopes that is deuterium, D:

$$X(D) = \frac{D}{H+D} \quad (2)$$

The random distribution of isotopologues is then derived by treating these fractional abundances as probabilities such that:

$$\begin{aligned} X(^{12}CH_4) &= X(^{12}C)(X(H))^4 \\ X(^{13}CH_4) &= X(^{13}C)(X(H))^4 \\ X(^{12}CH_3D) &= 4X(^{12}C)(X(H))^3X(D) \\ X(^{13}CH_3D) &= 4X(^{13}C)(X(H))^3X(D) \\ &\vdots \\ X(^{13}CH_4) &= X(^{13}C)(X(D))^4 \end{aligned} \quad (3)$$

where multiplicity from isotopomer abundances are accounted for (e.g., four possible positions for D substitution for four H positions leads to the exponents of 4 shown in Eqs. (3)) but are not written explicitly in what follows to simplify the presentation. Exchange of isotopes between isotopologues occurs by reactions such as

$$^{13}CH_4 + {}^{12}CH_3D \rightleftharpoons {}^{12}CH_4 + {}^{13}CH_3D \quad (4)$$

The equilibrium constant for this reaction is

$$k_{Eq} = \frac{[^{13}CH_3D][^{12}CH_4]}{[^{13}CH_4][^{12}CH_3D]} \quad (5)$$

where the square brackets denote concentrations that can be equated with the fractional abundances like those in Eqs. (3). At high temperatures (≥1000 K) the distributions of isotopologues are effectively random and substitution of the fractional abundances in Eqs. (3) into the equilibrium constant in Eq. (5) yields

$$\begin{aligned} k_{Eq,Stoch} &= \frac{[^{13}CH_3D][^{12}CH_4]}{[^{13}CH_4][^{12}CH_3D]} \\ &= \frac{4X(^{13}C)(X(H))^3X(D)X(^{12}C)(X(H))^4}{4X(^{12}C)(X(H))^3X(D)X(^{13}C)(X(H))^4} = 1 \end{aligned} \quad (6)$$

An equilibrium constant of unity in this case corresponds to a purely random distribution of isotopes among the molecules. At lower temperatures the stabilizing effects of two heavy isotopes bonded together begin to take hold and the equilibrium constant in Eq. (5) gets progressively larger as T goes down. This enhancement in rare multiply-substituted isotopologues, or clumping, is expressed in delta notation as

$$\Delta^{13}CH_3D = 10^3 \ln\left(\frac{k_{Eq}}{k_{Eq,Stochastic}}\right) \sim 10^3\left(\frac{X_{^{13}CH_3D}}{X_{^{13}CH_3D,Stochastic}} - 1\right) \quad (7)$$

Analogous expressions can be written for $^{12}CH_2D_2$. Both of these rare isotopologues have integer masses of 18. The two parameters $\Delta^{13}CH_3D$ and $\Delta^{12}CH_2D_2$ can serve as intra-molecular thermometers. The relationship between temperature and both $\Delta^{13}CH_3D$ and $\Delta^{12}CH_2D_2$ is readily calculated and is shown in Fig. 2. These results were obtained using ab initio calculations by Prof. Edwin Schauble at UCLA. Similar results were published by Ma et al. [21]. The calculation shows that variations in the concentration of the doubly-substituted isotopologues are expected to vary by several per mil over the ranges in temperature applicable to methane production. The relationship between $\Delta(^{13}CH_3D + \Delta^{12}CH_2D_2)$ vs. temperature has been confirmed recently through laboratory experiments [15].

Until now, measurements have been made spectroscopically for $\Delta^{13}CH_3D$ [22] or for the two mass-18 species combined, $\Delta(^{13}CH_3D + \Delta^{12}CH_2D_2)$ [15] due to the mass spectrometry limitations that have prevented separate measurements of the two species.

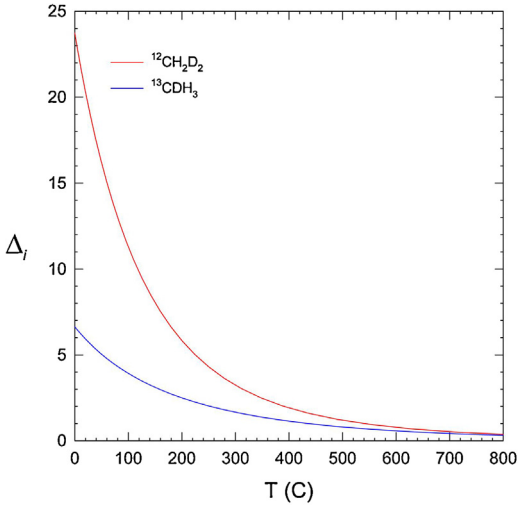

Fig. 2. Ab initio calculations for the temperature-dependence of $m = 18$ isotopologue excesses in CH_4 (calculations by E. Schauble).

The masses of $^{13}CH_3D$ and $^{12}CH_2D_2$ are 18.04094 and 18.04386 Da, respectively. Separating these species is challenging from the analytical perspective as it requires a mass resolving power of several times the $m/\Delta m$ of ~6000. What is worse, ion beams from $^{13}CH_5$ (18.04248 amu) and $^{12}CDH_4$ (18.045402 amu), both formed by ion-molecule reactions in the electron-impact source as a function of the square of source pressure, fall to either side of $^{12}CH_2D_2$ in the mass spectrum with $m/\Delta m$ of 13,132 and 11,6456, respectively. The minimum MRP for an interference-free measurement of $^{12}CH_2D_2$ is therefore of order 39,000 (3× 13,000). The low relative abundance of $^{12}CH_2D_2$ of 1.33×10^{-7} makes the measurement all the more challenging. Nonetheless, achieving this separation will greatly increase the information content in a sample of methane gas, extending far beyond ascertaining the temperature of formation alone.

As a simple example we consider the case of mixing (e.g., [20]) of CH_4 gases with different bulk isotopic compositions, one with $\delta^{13}C$ of −60‰ relative to the PDB standard ($\delta^{13}C_{PDB} = 10^3((([^{13}CH_4]/[^{12}CH_4])/([^{13}CH_4]/[^{12}CH_4])_{PDB} - 1))$ and $\delta D = -350‰$ relative to the SMOW standard ($\delta D_{SMOW} = 10^3((([^{12}CH_3D]/[^{12}CH_4])/([^{12}CH_3D]/[^{12}CH_4])_{SMOW} - 1))$, similar to a methane of microbial origin, and the other with $\delta^{13}C$ and δD values of −15 and −100‰, respectively, resembling a thermogenic methane with a very high $^{13}C/^{12}C$. For this illustration both gases will be assigned stochastic distributions of isotopologues, as if they both formed at high temperatures exceeding 1000 K. In this case the fractional abundance of $^{13}CH_3D$ for the "thermogenic" gas composition is

$$X(^{13}CH_3D)_{Thermo} = 6.135 \times 10^{-6} \quad (8)$$

and the fractional abundance of this species for the "methanogenic" gas is

$$X(^{13}CH_3D)_{Microb} = 4.231 \times 10^{-6} \quad (9)$$

We can calculate the expected stochastic abundance of $^{13}CH_3D$ for a gas with the bulk $^{13}C/^{12}C$ and D/H composition like that of a 50:50 mixture of these two gases, yielding

$$X(^{13}CH_3D)_{50:50\,Mix,\,Stochastic} = 5.164 \times 10^{-6} \quad (10)$$

However, simply mixing the two gases together does not involve bond rupture and formation and so the molecules retain the bond ordering (pairings of ^{13}C and D) established during their original

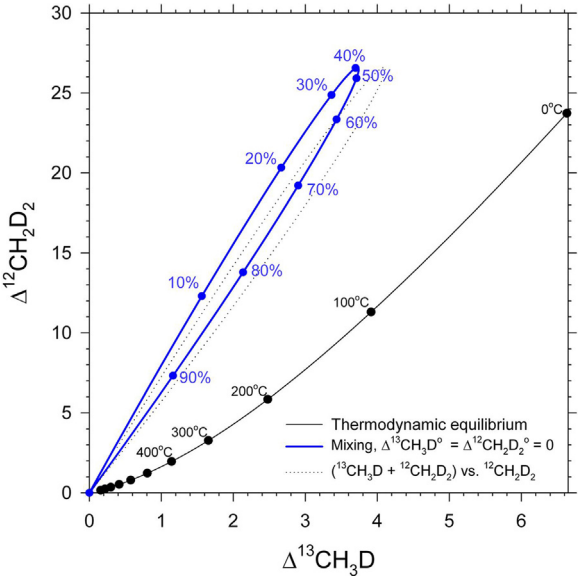

Fig. 3. Plot of excesses in $^{12}CH_2D_2$ and $^{13}CH_3D$ for mixtures of two stochastic CH_4 gases (blue curve) compared with gases in thermodynamic equilibrium (black curve). Dotted curve shows abscissa values where the two isotopologues are summed (i.e., not resolved)

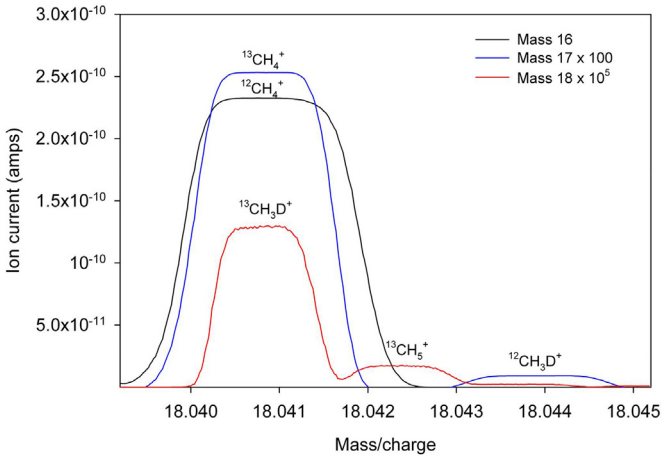

Fig. 4. Mass scan showing ion beam peaks for methane and interfering species. In this configuration the collector slits for cup L5 are set so that $^{12}CH_4^+$ is coincident with $^{13}CH_4^+$ and $^{13}CH_3D^+$. The abscissa gives the m/z for the axial position. The ordinate is ion current in amp for mass.charge 16. Intensities of the minor beams are scaled for presentation. In this scan the collector slit width for the axial secondary electron multiplier is optimized for $^{13}CH_3D^+$ and is wider than that used for $^{12}CH_2D_2{}^+$.

formation. As a result, the physical mixture has an observed fractional abundance of $^{13}CH_3D$ different from that in Eq. (10):

$$\frac{1}{2}X(^{13}CH_3D)_{Thermo} + \frac{1}{2}X(^{13}CH_3D)_{Microb} = 5.183 \times 10^{-6} \quad (11)$$

as the reader can verify from Eqs. (8) and (9). Simple mixing leads to an apparent equilibrium constant greater than unity:

$$k_{Eq,Apparent} = 1.00377 \quad (12)$$

despite the fact that both gases formed with stochastic distributions of isotopologues. This apparent equilibrium constant manifests as an excess in $^{13}CH_3D$ relative to stochastic:

$$\Delta^{13}CH_3D = 10^3 \ln\left(\frac{k_{Eq,Apparent}}{k_{Eq,Stochastic}}\right) = 3.71 \quad (13)$$

that implies a spurious temperature of formation of 110 °C. With no a priori knowledge that the gas sample was a mixture, measurements of $\Delta^{13}CH_3D$ alone would lead to the conclusion that the gas formed at 110 °C. However, by measuring *both* $\Delta^{13}CH_3D$ and $\Delta^{12}CH_2D_2$ separately, the mixing is evidenced by departures from expectations from thermodynamic equilibrium. This is shown in Fig. 3 where mixtures of these two stochastic gases are compared with gases in thermodynamic equilibrium at various temperatures. The loop represents mixtures and is labeled with per cent values of mixing. The single curve is the loci of gas compositions in thermodynamic equilibrium labeled with temperatures of equilibration. By measuring both $\Delta^{13}CH_3D$ and $\Delta^{12}CH_2D_2$ the presence of mixing is evident by excesses in $^{12}CH_2D_2$ relative to $^{13}CH_3D$ (i.e., the blue curve is above the black curve). Without measuring $^{12}CH_2D_2$ separately from $^{13}CH_3D$, we would misinterpret $\Delta^{13}CH_3D$ or $\Delta(^{13}CH_3D + \Delta^{12}CH_2D_2)$ (the latter approximates the former because in general $^{13}CH_3D \gg {}^{12}CH_2D_2$ in abundance), the abscissa values in Fig. 3, as indicating temperatures of formation that have nothing to do with the actual temperatures of formation of the gases comprising the mixture.

These mixing calculations are just one example of how deviations from thermodynamic distributions of the rare isotopologues can arise. Others include kinetics of reactions and transport by diffusion. In all such cases, measuring the relative abundance of the more abundant $^{13}CH_3D$ without measuring the abundance of $^{12}CH_2D_2$ can lead to misleading results.

3.2. Measuring CH_4 isotopologue ratios with the Panorama

The collectors are distributed in the Panorama as follows: two high-mass Faraday collectors, H2 and H1, an axial Faraday cup or electron multiplier, depending on the configuration, and six lower-mass Faraday collectors L1–L6 with L1 being closest to the axial position. Three collectors are utilized to measure CH_4 ion beams simultaneously. The species to be measured in studies of the mass-18 rare isotopologues of methane include $^{12}CH_4^+$ (integer mass 16 in Faraday cup L5), $^{13}CH_4^+$ (mass 17 in Faraday cup L3), $^{12}CH_3D^+$ (mass 17 in Faraday cup L3), $^{13}CH_3D^+$ (mass 18 in the axial ion counter) and $^{12}CH_2D_2{}^+$ (mass 18 in the axial ion counter). As described above, resolving interferences from various CH_5 species produced in the source requires an MRP of ~39,000 or greater. The mass spectrum for methane gas obtained with the Panorama is shown in Fig. 4.

The isotopologue ratio measurements are obtained at two magnet settings. In the first setting, shown in Fig. 4, the magnet is set to collect $^{13}CH_3D^+$ (integer mass 18, actual mass 18.0409) in the axial position and $^{13}CH_4^+$ (mass 17) in L3, and the independently variable L5 collector slits are set for coincidence of the $^{12}CH_4^+$ (mass 16) peak flat, yielding simultaneous measurement of $^{13}CH_4/{}^{12}CH_4$ and $^{13}CH_3D/{}^{12}CH_4$ ratios. At an MRP of ~40,000, interference on $^{13}CH_3D^+$ from $^{13}CH_5^+$ is easily resolved (Fig. 4). Mass resolving power for the axial ion counter at two different entrance slit settings is shown in Fig. 5, illustrating the typical resolution of the Panorama for these types of measurements. At an MRP of ~47,000, interference from $^{12}CHD_2{}^+$ on $^{13}CH_4^+$ (mass 17) is resolved. The former is normally below detection. However, we demonstrated the ability to resolve the fragment $^{12}CHD_2{}^+$ from $^{13}CH_4^+$ by measuring a methane sample spiked with per cent levels of CH_2D_2 (Fig. 6). The mass resolving power is lower further from the axial beam. For an axial MRP of ~47,000, the MRP for the off-axis L3 cup is about 38,000.

In the second setting, the magnet current is set to collect $^{12}CH_2D_2{}^+$ (integer mass 18, actual mass 18.04385) in the axial ion counter and $^{12}CH_3D^+$ (mass 17) in L3, and the collector slits for L5 are shifted to place the $^{12}CH_4^+$ beam (mass 16) peak flat

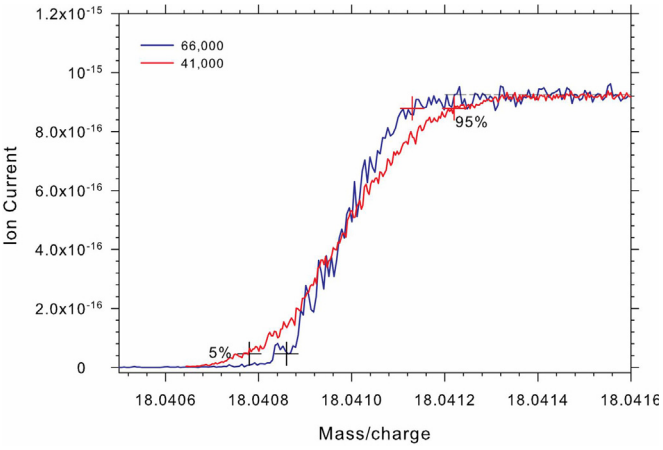

Fig. 5. Mass resolving power measured on the $^{13}CH_3D^+$ beam in the axial ion counter. Two different settings for the entrance slit are shown, corresponding to MRP of 66,000 and 41,000 using the 5–95% peak height definition. The nominal entrance slit widths for the two settings are 21 and 34 μm, respectively.

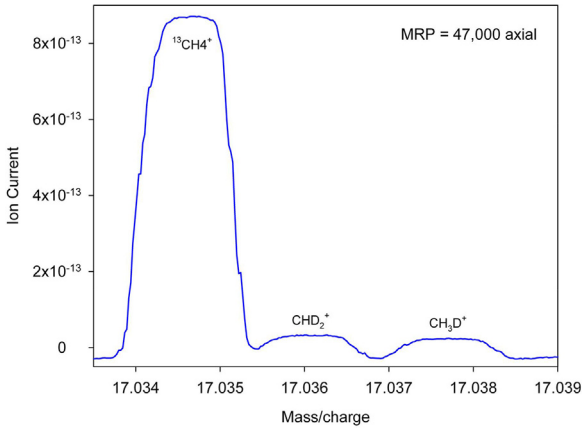

Fig. 6. Mass scan showing separation of mass-17 species. The peak-to-peak mass resolution is ~12,000 (i.e., $M/\Delta M$ where ΔM is from peak center to peak center).

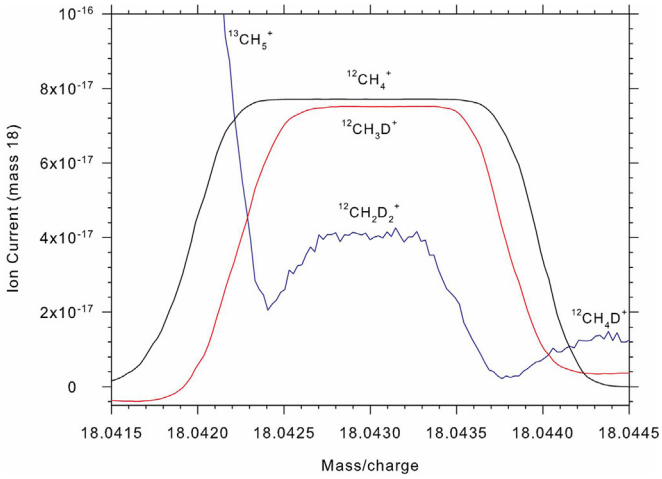

Fig. 7. Methane peak shapes in the second magnet setting for measurement of $^{12}CH_3D^+/^{12}CH_4^+$ and $^{12}CH_2D_2^+/^{12}CH_4^+$. Mass/charge and ion current refer to the axial collector. Ion currents for the other cups are scaled for comparison with the axial ion counter.

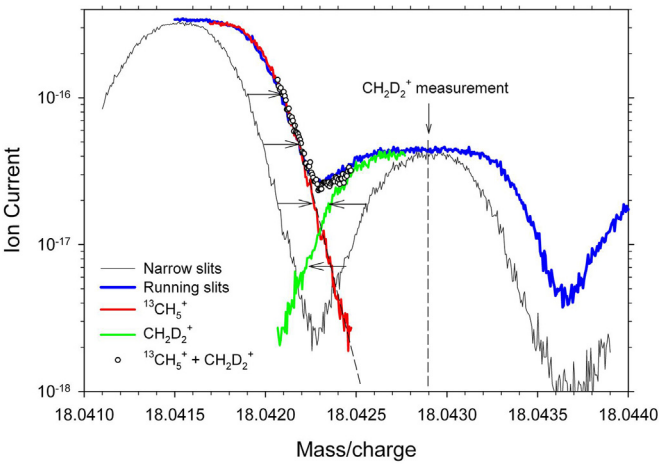

Fig. 8. Comparison of mass-18 ion peak shapes for two collector slit settings. Narrow black line shows the peak shapes for $^{13}CH_5^+$ and $^{12}CH_2D_2^+$ with a narrow collector slit. The thicker blue line shows the partially overlapping peaks with a wider collector slit setting. The limbs of the peaks for the wider setting are simulated by migrating those from the narrower-slit scan to appropriate positions along the abscissa (red and yellow lines for $^{13}CH_5^+$ and $^{12}CH_2D_2^+$, respectively). The open circles are the sum of the migrated limbs. The match between the sum and the actual wider-slit data validates the construction. Data were collected using the axial secondary electron multiplier with count rate converted to ion current in amp.

coincident with the $^{12}CH_3D^+$ and $^{12}CH_2D_2^+$ ion beams. This configuration is shown in Fig. 7 where it can be seen that $^{12}CH_2D_2^+$ is resolved from $^{13}CH_5^+$ on the low-mass side and $^{12}CH_4D^+$ on the high mass side. In this configuration the $^{12}CH_3D/^{12}CH_4$ and $^{12}CH_2D_2/^{12}CH_4$ ratios are obtained simultaneously. The width of the $^{12}CH_2D_2^+$ peak flat in Fig. 7 is 27 ppm and is more than adequate for isotope ratio measurements. The MRP is optimized to avoid the influence of the neighboring $^{13}CH_5^+$ tail on the measured $^{12}CH_2D_2^+$ peak. The relative size of the $^{13}CH_5^+$ beam (and that of all of the CH_5^+ species) depends on the square of the gas pressure since it forms from a bimolecular reaction in the source. The ratio of CH_5^+ to $^{12}CH_2D_2^+$ can therefore be controlled by the flow rate through the crimped capillaries to the source.

We can illustrate the sensitivity of the measured $^{12}CH_2D_2^+$ ion beam intensity to the $^{13}CH_5^+$ tail by comparing mass scans with relatively narrow and relatively wide axial collector slit widths. Fig. 8 shows a reconstruction of the overlapping $^{12}CH_2D_2^+$ and $^{13}CH_5^+$ peak limbs for an unusually wide collector-slit setting based on the peak shapes obtained with the collector slit more closed. The wide slit peak shape in Fig. 8 is in effect a worst-case scenario (compare with peak shapes in Fig. 7). Extrapolation of the $^{13}CH_5^+$ peak tail in Fig. 8 to the 18.04249 amu peak center for $^{12}CH_2D_2^+$ yields a 0.3‰ contribution to the ion current. The effects of this tail component are mitigated by normalizing to the reference gas using the dual inlet. Using the example in Fig. 8, we can compute the effect of adding the 0.3‰ ion current representing the $^{13}CH_5^+$ tail beneath the $CH_2D_2^+$ ion currents for reference and sample gases because the $^{13}CH_5^+$ tail scales with the major beam intensity (i.e., source gas pressure). In the case of a sample gas that is 800‰ higher in δCH_2D_2 than the reference gas (or roughly 400‰ higher in bulk D/H, representing an extreme for natural samples), the presence of the tail alters the typical $CH_2D_2^+$ ion current from 4.000000×10^{-17} to 4.001202×10^{-17} amp for the reference gas and from 7.200000×10^{-17} to 7.201202×10^{-17} amp for the sample gas. The result on the δCH_2D_2 is a spurious shift of −0.24‰. At a δCH_2D_2 of 500‰ the tail effect is −0.15‰. These calculations demonstrate that the effect of tailing is less than the internal precision limitations on δCH_2D_2 from counting statistics (~0.5‰, see below) for natural D/H abundances. Corrections would be warranted in those cases where the axial collector slits are significantly wider than in Fig. 8 for example, and where bulk D/H of the sample

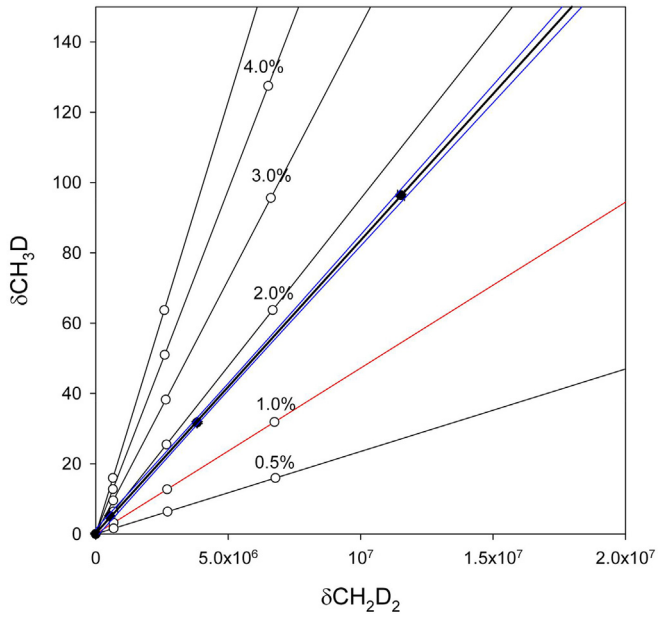

Fig. 9. Plot of $^{12}CH_2D_2/^{12}CH_4$ (abscissa) and $^{12}CH_3D/^{12}CH_4$ (ordinate) for gases with different concentrations of CH_2D_2 spike (black symbols) measured on the Panorama compared with predictions for isotopic bond reordering (open circles). Black lines are isopleths for different degrees of reordering in per cent. The heavy black line with 95% error envelope (blue lines) is the regression of the measurements.

gas is hundreds of per mil disparate from the reference gas. Under our usual operating conditions (e.g., Fig. 7), such a correction is not warranted.

3.3. Fidelity of isotope bond ordering in the electron-impact source

When the goal is to obtain the relative abundances of doubly-substituted isotopologues, the potential for disturbing the sample bond ordering by breaking and reforming bonds in the electron-impact source must be evaluated. We did this by measuring samples of methane gas spiked with various concentrations of CH_2D_2 (≥98% CH_2D_2 from Cambridge Isotope Laboratories, Lot No. Pr-18207) following the procedure previously used for O_2 [7]. In these tests, we look for the conversion of $^{12}CH_2D_2$ to $^{12}CH_3D$ in the source of the instrument by a net reaction such as

$$CH_2D_2 + CH_4^+ \rightarrow 2CH_3D^+ + e^- \quad (14)$$

as measured by downward shifts in $^{12}CH_2D_2/^{12}CH_4$ reported in per mil as $\delta CH_2D_2 = 10^3((([^{12}CH_2D_2]/[^{12}CH_4])/([^{12}CH_2D_2]/[^{12}CH_4])_o - 1)$ and upward shifts in $^{12}CH_3D/^{12}CH_4$ reported as $\delta CH_3D = 10^3((([^{12}CH_3D]/[^{12}CH_4])/([^{12}CH_3D]/[^{12}CH_4])_o - 1)$ where the subscripted zero indicates the original isotopologue ratio prior to progress of reaction (14). In practice, the relative shifts in δCH_2D_2 will be small with isotopic bond reordering while the relative shifts in δCH_3D will be larger; large shifts in δCH_3D are diagnostic of progress of reactions like (13). For example, a sample gas with 3% $^{12}CH_2D_2$ spike will shift from an original isotopic composition with $\delta CH_3D = 0.0‰$ and $\delta CH_2D_2 = 6.812 \times 10^6$ to one with δCH_3D of 15.8‰ and δCH_2D_2 of 6.786×10^6‰ with 0.5% progress of reaction (14) (Fig. 9).

Results of our tests using various spike concentrations are shown in Fig. 9. They demonstrate that the degree of isotopic bond reordering in the Panorama source is slightly less than 2%. In most cases this degree of scrambling will be within measurement uncertainties. The scrambling value of ~2% is similar to the 1.1% value

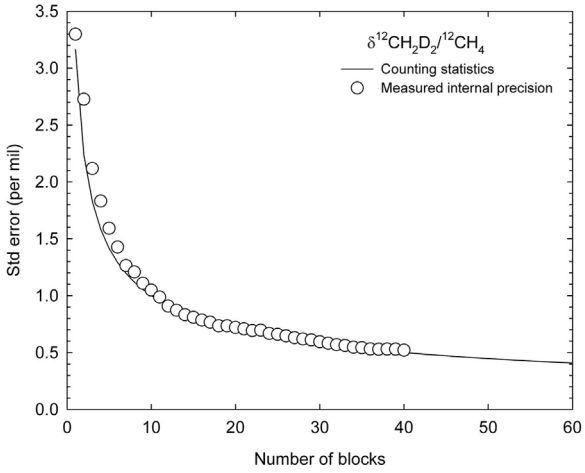

Fig. 10. Internal precision as a function of number of 20 std-smpl-std measurement blocks. The curve shows the prediction based on counting statistics alone. The open symbols show a measurement made over a 26-h interval. The $^{12}CH_2D_2^+$ ion beam was measured on the secondary electron multiplier at a count rate of ~250 cps for this example.

obtained for O_2 in a smaller-geometry gas-source IRMS [7] and may be typical for many gases in electron-impact sources in general. Experiments were run at different source repeller voltages with no deviation from the linear relationship in Fig. 9. Different repeller settings result in different intensities of the CH_5^+ molecule because repeller voltage controls the residence time in the source. Our finding that the repeller has no resolvable influence on scrambling indicates that the 2% scrambling is robust.

3.4. Internal precision

A key performance parameter is the precision with which measurements can be made using the secondary electron multiplier on the Panorama. The most stringent test is the precision for $^{12}CH_2D_2/^{12}CH_4$ determinations because of the low abundance of the doubly-deuterated species. We find that the measurement internal precision generally follows counting statistics where the internal precision is the cumulative standard error (1σ error in the mean) of $\delta^{12}CH_2D_2$ values (per mil differences in $^{12}CH_2D_2/^{12}CH_4$ of the sample relative to the standard gas) for all of the blocks of standard-sample-standard comparisons. For example, in Fig. 10 we compare the precision expected from counting statistics alone as a function of number of blocks of 20 $\delta^{12}CH_2D_2$ determinations with the measured standard error for $\delta^{12}CH_2D_2$ obtained from an analysis of methane gas relative to our in-house reference gas. For these measurements each block consists of twenty 30-s sample integrations and 21 standard-gas integrations. The ion currents for the measurements and calculations in Fig. 10 are $\sim 4.0 \times 10^{-17}$ amp (~250 counts per second on the ion counter) and $\sim 4.5 \times 10^{-10}$ amp for the $^{12}CH_2D_2^+$ and $^{12}CH_4^+$ beams, respectively. The agreement between the internal precision and that predicted from counting statistics alone indicates that the instrument is well optimized and stable over the 26 h required to obtain 40 blocks. A 40-block measurement yields ~0.5‰ precision for $\delta^{12}CH_2D_2$. The internal-precision uncertainties for the other isotopologue ratios are all considerably smaller (Table 1).

3.5. Accuracy

We measured several methane gas samples from the laboratories at MIT (Shuhei Ono and team, pers. comm.) and University of Toronto (Barbara Sherwood Lollar and team, pers. comm.) for which isotopologue ratios are considered to be well characterized. The

Table 1
Comparisons between accepted isotopic compositions and measurements made with the Panorama large-radius gas-source multiple-collector mass spectrometer. PDB refers to the Pee Dee Belemnite carbonate standard and SMOW refers to the Standard Mean Ocean Water standard. All values are in per mil relative to the indicated standard.

	Measured		Accepted		Measured		Accepted		Measured		Accepted		Measured		Accepted
Gas	$\delta^{13}C_{PDB}$	se	$\delta^{13}C_{PDB}$	±	δD_{SMOW}	se	δD_{SMOW}	±	$\Delta^{13}CH_3D$	se	$\Delta^{13}CH_3D$	±	$\Delta^{12}CH_2D_2$	se	$\Delta^{12}CH_2D_2$
MIT AL-1 (1)	−34.647	0.006	−34.5	0.25	−147.881	0.093	−147.7	2.5	2.413	0.262	2.41	0.07	5.624	0.865	5.53[a]
MIT AL-1 (2)	−34.483	0.003	−34.5	0.25	−148.236	0.012	−147.7	2.5	2.410	0.142	2.41	0.07	5.598	0.35	5.53[a]
MIT AL-1 CD	−82.006	0.033	−81.97	0.03	−159.715	0.03	−159.37	0.03	16.134	0.303	16	0.2	–	–	–
MIT AL-1 D3	−34.759	0.003	−34.52	0.04	242.548	0.011	242.84	0.04	1.545	0.124	0.9	0.2	–	–	–
SIL 59	−42.203	0.033	−42.3	0.2	−67.757	0.429	−66	4	–	–	–	–	–	–	–
SIL 60 (1)	−41.073	0.01	−41.4	0.2	−168.848	0.04	−165	1	–	–	–	–	–	–	–
SIL 60 (2)	−41.129	0.023	−41.4	0.2	−169.017	0.04	−165	1	–	–	–	–	–	–	–
Indiana 1	−38.167	0.032	−38.25	0.03	−161.353	0.057	−161	2.1	–	–	–	–	–	–	–
Indiana 2	−37.467	0.008	−37.6	0.03	−45.295	0.189	−41	1.3	–	–	–	–	–	–	–

[a] Based on assumed equilibration temperature of 208.8 °C.

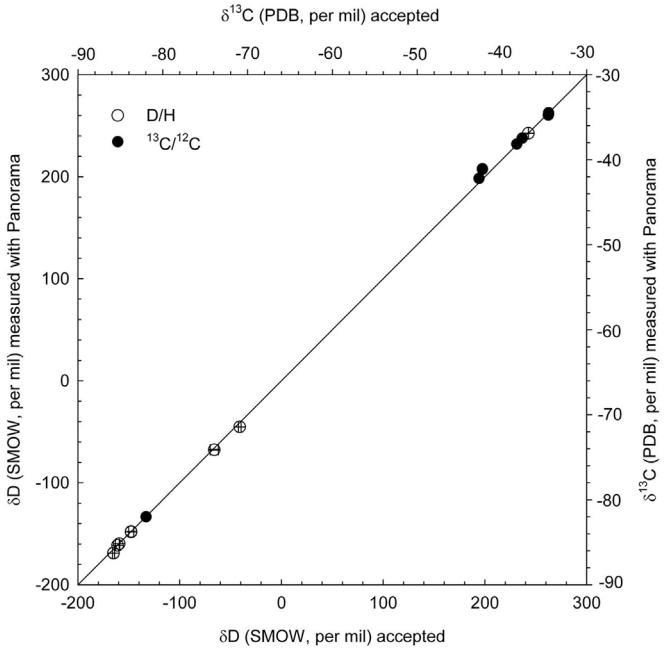

Fig. 11. Plots of measured vs. accepted δD relative to SMOW (open symbols) and $\delta^{13}C$ relative to PDB (closed symbols). Axis labels for δD are on the left and bottom. Axis labels for $\delta^{13}C$ are on the right and top. Where error bars (as in Table 1) are not visible, they are smaller than the symbols. A 1:1 line is shown for reference.

Toronto samples provide estimates of accuracy for bulk $^{13}C/^{12}C$ and D/H relative to standard mass spectrometry methods. The MIT samples provide an opportunity to compare our measured $\Delta^{13}CH_3D$ with values obtained by tunable infrared laser direct-absorption spectroscopy (TILDAS) [22]. The latter is the only other method for measuring $\Delta^{13}CH_3D$ free from mixing with $^{12}CH_2D_2$ ions. Results are given in Table 1 and Fig. 11. Our δD_{SMOW} and $\delta^{13}C_{PDB}$ values generally agree within uncertainties with the Toronto and MIT laboratories (Fig. 11), and the internal precision of the δD_{SMOW} measurements of ≪0.1‰ is about an order of magnitude better than that obtained from traditional methods. One reason for this improvement in precision is no doubt that we are measuring the bulk D/H on the methane directly without the conversion to hydrogen gas required by traditional methods on lower-resolution mass spectrometers where mass-17 isotopologues cannot be resolved. Another is the very long counting times used in order to achieve requisite precision for $^{12}CH_2D_2/^{12}CH_4$.

Our $\Delta^{13}CH_3D$ measurement for the MIT AL-1 gas agrees with the TILDAS measurements to better than 0.1‰ (Table 1). There are currently no measurements of $\Delta^{12}CH_2D_2$ at natural abundances available with which to compare. However, if we assume that the AL-1 gas is in thermal equilibrium with respect to isotopic bond ordering, then the $\Delta^{13}CH_3D$ value of 2.41 suggests a temperature of 208.8 °C that in turn suggests a $\Delta^{12}CH_2D_2$ value of 5.53‰ that matches well our measured values of 5.6 ± 0.9 and 5.6 ± 0.4‰ (the first measurement made with lower ion current than the second measurement).

3.6. Mixing experiments

Two methane gas samples were mixed together in various proportions in order to demonstrate the accuracy and precision of the $^{13}CH_3D/^{12}CH_4$ and $^{12}CH_2D_2/^{12}CH_4$ measurements. The isotopic compositions of the two gases differ by 4.21‰ in $\delta^{13}C_{PDB}$ and 119‰ in δD_{SMOW} (Table 2). As described in Section 3.1, mixing of gases of different bulk isotopic compositions without bond rupture and reformation leads to departures from the thermodynamic equilibrium in plots of $\Delta^{13}CH_3D$ vs. $\Delta^{12}CH_2D_2$, and we should see this calculable departure in the results. These experiments serve as one test of the efficacy of the Panorama instrument in resolving interferences.

Gases were mixed in the dual inlet of the mass spectrometer by equilibrating for ∼1 h while actively moving the gas with the variable volume bellows. Results are tabulated in Table 2 and shown in Fig. 12. The data adhere to the predicted mixing curve within uncertainties. They demonstrate that as little as 10% mixing between gases with these disparate bulk isotopic compositions can be detected.

The gases shown in Fig. 12 and listed in Table 2 were placed on an absolute scale assuming that MIT AL-1 is exactly correct in $\Delta^{13}CH_3D$ and that this gas is in thermodynamic equilibrium with respect to bond ordering. The assessment of accuracy afforded by the mixing experiment is independent of this assumption as it tests the relative differences between the gases.

4. Other applications

There are a large number of applications for which the large-radius gas-source instrument could be a benefit. These applications are made possible by the combination of movable collectors and independently movable collector slits that provide flexibility in designating analytes. As examples, we have performed preliminary analyses of N_2 and O_2 multiply-substituted isotopologues as described below. Results from the studies involving these gases will be presented elsewhere, but the capabilities of the instrument for resolving the multiply-substituted isotopologues of interest are discussed in what follows.

4.1. $^{15}N^{15}N$

The relative abundance of $^{15}N^{15}N$ in N_2 gas holds promise as a tracer for the nitrogen budget of the atmosphere and the global

Table 2
Results of methane mixing experiments.

Mixing ratio UCLA-2	δ^{13}CPDB	Std err	δD_{SMOW}	Std err	$\Delta^{13}CH_3D$	Std err	$\Delta^{12}CH_2D_2$	Std err
0.00	−40.911	–	−178.017	–	2.903	–	7.257	–
0.11	−40.453	0.004	−165.254	0.012	2.631	0.127	8.61	0.475
0.18	−40.094	0.013	−156.103	0.012	2.334	0.122	8.858	0.475
0.28	−39.753	0.004	−144.851	0.0109	2.183	0.109	9.078	0.47
0.35	−39.455	0.005	−136.590	0.012	2.127	0.123	8.628	0.457
0.45	−39.000	0.008	−124.485	0.012	1.79	0.113	8.691	0.49
0.55	−38.630	0.005	−113.066	0.015	1.453	0.105	7.364	0.503
0.62	−38.365	0.006	−104.855	0.014	1.255	0.134	6.115	0.663
0.74	−37.650	0.022	−90.705	0.017	1.059	0.128	5.077	0.52
0.89	−37.111	0.006	−71.463	0.013	0.403	0.117	1.921	0.569
1.00	−36.631	0.021	−59.121	0.018	0.351	0.024	0.412	0.551

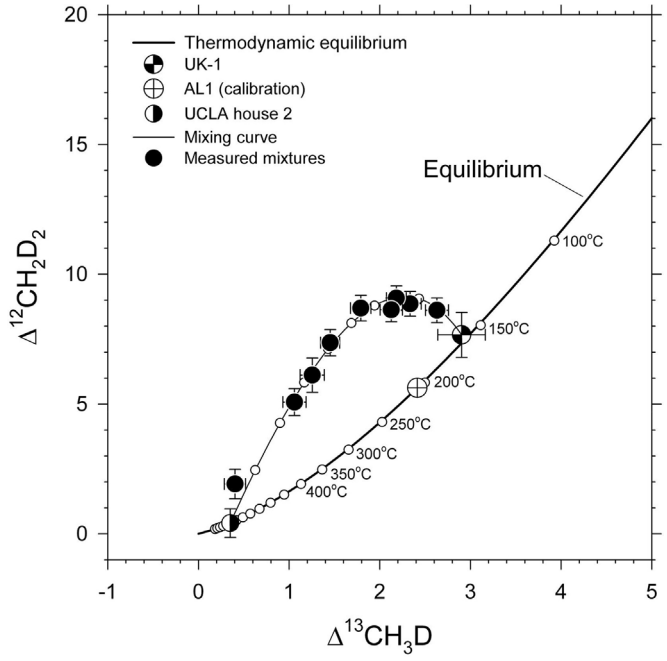

Fig. 12. Results of mixing experiments (black symbols) compared with the curve depicting thermodynamic equilibrium, marked with temperatures, and the predicted mixing curve. Dots on the mixing curve represent 10% intervals for mixing ratios. Error bars are 1 std error (1σ in the mean) for each datum.

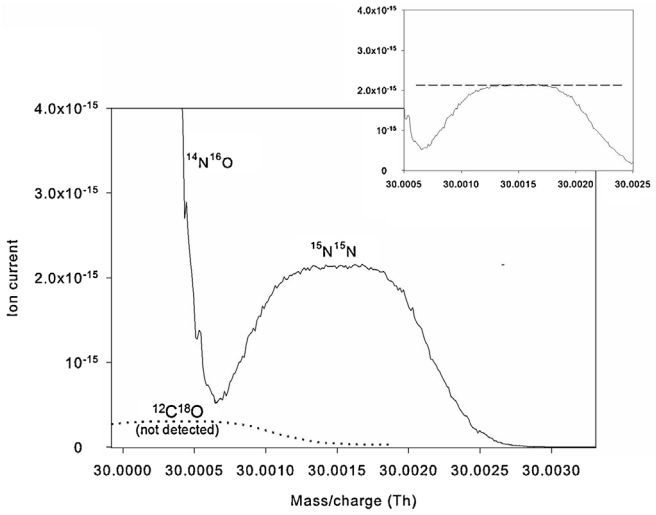

Fig. 13. Mass scan showing separation of $^{30}NO^+$ from $^{30}N_2{}^+$ in the Panorama instrument. Inset shows a magnified view of the $^{15}N^{15}N$ peak shape with a horizontal line depicting the peak flat. The scan represents multiple integrations using the secondary electron multiplier with count rate converted to current. The dotted line shows the predicted position and shape of the $^{30}CO^+$ peak, at an arbitrary fictive ion current. This species has not yet been observed at higher resolution.

nitrogen budget as a whole. Measurements of the $^{30}N_2/^{28}N_2$ ratio on conventional small-geometry gas-source IRMS instruments are precluded by interferences from $^{30}NO^+$ ($^{14}N^{16}O^+ + ^{16}O^{14}N^+$) produced in the electron-impact sources and trace amounts of CO^+ where present. Interferences for $^{28}N_2{}^+$ ($^{14}N^{14}N^+$) and $^{29}N_2{}^+$ ($^{15}N^{14}N^+ + ^{14}N^{15}N^+$) from $^{28}CO^+$ ($^{12}C^{16}O^+ + ^{16}O^{12}C^+$) and $^{29}CO^+$ ($^{13}C^{16}O^+ + ^{16}O^{13}C^+ + ^{12}C^{17}O^+ + ^{17}O^{12}C^+$), respectively are easily resolved at the normal operating resolution of the Panorama; the $m/\Delta m$ separating $^{12}C^{16}O^+$ from $^{28}N_2{}^+$ is 2495, that separating $^{13}C^{16}O^+$ from $^{29}N_2{}^+$ is 5907, and that separating $^{12}C^{17}O^+$ from $^{29}N_2{}^+$ is 7163. These require mass resolving powers of at least 7500, 18,000, and 21,500, respectively, considerably less than the normal operating Panorama MRP of ~40,000.

Interferences on mass 30 are more challenging. The $m/\Delta m$ separating $^{30}NO^+$ from $^{30}N_2{}^+$ is 13,423, requiring an MRP of 40,270, matching the typical MRP employed with the Panorama. The $m/\Delta m$ separating $^{30}CO^+$ ($^{12}C^{18}O^+ + ^{18}O^{12}C^+$) from $^{30}N_2{}^+$ is 28,275, requiring an MRP of 85,000 based on the rule-of-thumb that MRP must approach $3 \times m/\Delta m$. The mass spectrum for the $^{30}N_2{}^+$ beam at the normal operating MRP of about 40,000 for the Panorama is shown in Fig. 13. The $^{30}N_2{}^+$ is resolved from $^{30}NO^+$ with a peak flat of about 13–16 ppm in this scan. While measurements can be made in this configuration, the collector slit can be widened somewhat in order to expand the peak flat without compromising the fidelity of the $^{30}N_2{}^+/^{28}N_2{}^+$ measurement in a manner analogous to that discussed in Section 3.2. Also shown in Fig. 13 is the predicted position and shape (with arbitrary peak height) of $^{30}CO^+$. However, this species has not been detected in N_2 gas samples even with narrower collector slits and MRPs of ~60,000 where the mass-30 species should be well separated. This observation is consistent with the absence of CO^+ in the mass-28 and mass-29 scans.

We have carried out analyses of $^{30}N_2{}^+/^{28}N_2{}^+$ and $^{29}N_2{}^+/^{28}N_2{}^+$ with internal precision of ±0.1–0.2‰ and ±0.005‰, respectively. There are no indications of spurious results from lingering mass interferences in these analyses. Results are being prepared for publication elsewhere.

4.2. $^{18}O^{18}O$

The relative abundance of the doubly-substituted diatomic oxygen species $^{36}O_2$ ($^{18}O^{18}O$) holds promise as a tracer of troposphere-stratosphere mixing [7,23] and as a marker for biological productivity [24]. Measurements of the relative abundance of this doubly-substituted oxygen molecule are hampered when using the typical smaller-geometry gas-source IRMS instruments because of the irresolvable interference from $^{36}Ar^+$ on $^{36}O_2{}^+$. This interference is severe even with purification of air samples by gas chromatographic separation of N_2, Ar and O_2 resulting in only 3 to 17 ppb ^{36}Ar in the purified O_2 [7]. Up until now, measurements

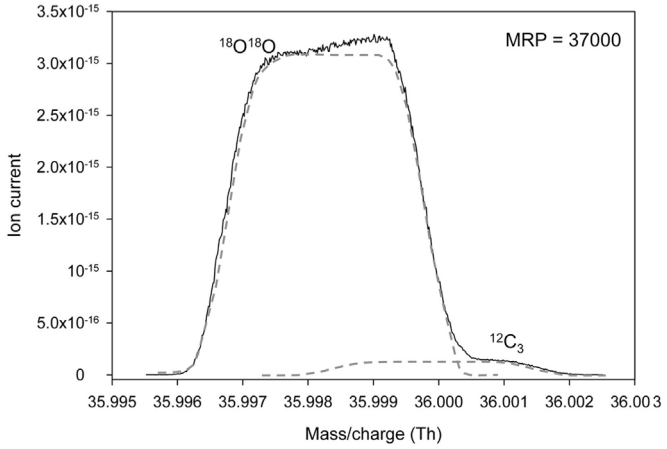

Fig. 14. Mass/charge scan showing the overlap between the $^{36}O_2^+$ ion beam at lower mass and the $^{12}C_3^+$ ion beam at higher mass. The contributions of the two ion beams to the total signal are sketched schematically using the dashed gray lines. $^{36}Ar^+$ and $H^{35}Cl^+$ lie far to the left off the diagram at 35.9675 Th and 35.9767 Th, respectively.

have been made by subtracting the substantial $^{36}Ar^+$ signal from $^{36}O_2^+$, significantly limiting the precision of the results [7].

The $m/\Delta m$ separating $^{36}Ar^+$ from $^{36}O_2^+$ is 1170 and so these species are easily resolved with the Panorama instrument. We were surprised to find that a major interference for $^{36}O_2^+$ also comes from ubiquitous $H^{35}Cl^+$. The $m/\Delta m$ in this case is only 1663 and so this species is also easily resolved from $^{36}O_2^+$. Another surprise, at least to us, is the presence of $^{12}C_3$ overlapping the $^{36}O_2^+$ peak at an MRP of 37,000 (Fig. 14). The $m/\Delta m$ between $^{12}C_3$ and $^{36}O_2^+$ is 21,430, suggesting that an MRP of ~60,000 is required for effective separation. The $^{36}O_2^+$ peak flat at MRP = 37,000 in Fig. 14 is about 8 ppm in width. Measurements on this flat are possible. However, a wider peak flat would be preferable. The collector slits can be reduced and the MRP improved to attain a reasonable condition for measurements long in duration and nearly free of $^{12}C_3$ interference. It appears that the $^{12}C_3$ interference is common to both sample and standard gases in the instrument, so complete elimination of the carbon species is probably not necessary for accurate $^{36}O_2/^{32}O_2$ measurements. Nonetheless, we can obtain a small peak flat on $^{36}O_2^+$ with an MRP of ~60,000. Future work will focus on balancing MRP between 40,000 and 60,000 and collector slit widths to define the best peak flat for these analyses. Thus far we have achieved an internal precision of ±0.06‰ for $^{36}O_2/^{32}O$.

5. Conclusions

The Panorama is the first large-radius gas-source multiple-collector isotope ratio mass spectrometer. It has mass resolving capabilities rivaling the largest multi-collector mass spectrometers. This new instrument makes it possible to measure the relative abundances of rare isotopologues of gaseous species with high transmission and effectively free from significant interfering species. The addition of continuous rebalancing to the Murphy–McKinney-type dual inlet improves the stability of analyses and extends the usable analysis time to several tens of hours. Relatively low count rates on the secondary electron multiplier can be utilized with long run times to achieve of order 0.1‰ precision. Applications to methane, oxygen, and nitrogen are underway. These and future applications have the potential to facilitate a new type of isotope chemistry based on isotopic bond-ordering.

Acknowledgements

Funding for the Panorama mass spectrometer has come from the Deep Carbon Observatory (Sloan Foundation), the National Science Foundation's EAR Instrumentation and Facilities Program, the Department of Energy Office of Science, The University of California Los Angeles, the Carnegie Institution of Washington, and Shell Projects and Technologies, Emerging Technologies Group. A large group of people contributed to the design and implementation, including Peter Li and David Rousell, among many others at Nu Instruments. Edwin Schuable (UCLA), Laurence Yeung (Rice University), Issaku Kohl (UCLA), Shuning Li (Rice University), and Jeanine Ash (UCLA) all contributed to this project at various times during development and installation of the instrument and analysis of samples. Barbara Sherwood Lollar and her group (University of Toronto) and Shuhei Ono and his group (MIT) kindly contributed samples for the first analyses of methane gas reported here.

References

[1] A.O. Nier, A mass spectrometer for isotope and gas analysis, Rev. Sci. Instrum. 18 (1947) 398–410.
[2] J.A. Hunter, R.W. Stacy, F.A. Hitchcock, A mass spectrometer for continuous gas analysis, Rev. Sci. Instrum. 20 (1949) 333–336.
[3] C.R. McKinney, et al., Improvements in mass spectrometers for the measurement of small differences in isotope abundance ratios, Rev. Sci. Instrum. 21 (1950) 724–730.
[4] B.F. Murphy, The temperature variation of thermal diffusion factors for binary mixtures of H, D and He, Phys. Rev. 72 (1947) 834–837.
[5] W.G. Cross, Two-directional focussing of charged particles with a sector-shaped, uniform magnetic field, Rev. Sci. Instrum. 22 (1951) 717–722.
[6] J.M. Eiler, "Clumped-isotope" geochemistry – the study of naturally-occurring, multiply substituted isotopologues, Earth Planet. Sci. Lett. 262 (2007) 309–327.
[7] L.Y. Yeung, E.D. Young, E.A. Schauble, Measurements of $^{18}O^{18}O$ and $^{17}O^{18}O$ in the atmosphere and the role of isotope-exchange reactions, J. Geophys. Res. (2012) 117, http://dx.doi.org/10.1029/2012JD017992.
[8] W. Compston, I.S. Williams, C. Meyer, Proceedings of the Fourteenth Lunar and Planetary Science Conference, 1984, pp. B525–B534.
[9] S. Clement, W. Compston, G. Newstead, Proceedings of the International Secondary Ion Mass Spectroscopy Conference, 1977.
[10] J.S. Becker, Recent developments in isotope analysis by advanced mass spectrometric techniques, J. Anal. At. Spectrom. 20 (2005) 1173–1184.
[11] A.J. Dempster, New methods in mass spectrometry, Proc. Am. Philos. Soc. 75 (1935) 755–767.
[12] A.O. Nier, A double-focussing mass spectrometer, Natl. Bureau Standards Circular (U.S.) 522 (1953) 29–36.
[13] E.G. Johnson, A.O. Nier, Angular aberrations in sector shaped electromagnetic lenses for focusing beams of charged particles, Phys. Rev. 91 (1953) 10–17.
[14] J.M. Eiler, et al., A high-resolution gas-source isotope ratio mass spectrometer, Int. J. Mass spectrom. 335 (2013) 45–56.
[15] D.A. Stolper, et al., Combined ^{13}C–D and D–D clumping in methane: methods and preliminary results, Geochem. Cosmochim. Acta 126 (2014) 169–191.
[16] F.P. Abramson, J.H. Futrell, Ion-molecule reactions of methane, J. Chem. Phys. 45 (1966) 1925–1931.
[17] H. Matusda, Double focusing mass spectrometers of second order, Int. J. Mass Spectrom. Ion Phys. 14 (1974) 219–233.
[18] M. Schuhmacher, et al., in: A. Benninghoven, et al. (Eds.), Secondary Ion Mass Spectrometry (SIMS IX), John Wiley & Sons, 1984, pp. 919–922.
[19] Z. Wang, E.A. Schauble, J.M. Eiler, Equilibrium thermodynamics of multiply substituted isotopologues of molecular gases, Geochim. Cosmochim. Acta 68 (2004) 4779–4797.
[20] J.M. Eiler, E. Schauble, $^{18}O^{13}C^{16}O$ in Earth's atmosphere, Geochim. Cosmochim. Acta 68 (2004) 4767–4777.
[21] Q. Ma, S. Wu, Y. Tang, Formation and abundance of doubly-substituted methane isotopologues ($^{13}CH_3D$) in natural gas systems, Geochem. Cosmochim. Acta 72 (2008) 5446–5456.
[22] S. Ono, et al., Measurement of a doubly substituted methane isotopologue, $^{13}CH_3D$, by tunable infrared laser direct absorption spectroscopy, Anal. Chem. 86 (2014) 6487–6494.
[23] L.Y. Yeung, J.L. Ash, E.D. Young, Rapid photochemical equilibration of isotope bond ordering in O_2, J. Geophys. Res. Atmos. 119 (2014) 15.
[24] L.Y. Yeung, J.L. Ash, E.D. Young, Biological signatures in clumped isotopes of O_2, Science 348 (2015) 431–434.